symmetry

MDPI

Article

Enhanced Intentional Controlled Islanding in Power Systems Using Constrained Spectral Clustering with Data Amelioration and Dynamic Validation

Francisco Rivas-Dávalos [1,*], Paulina García-Peña [1], Eduardo Cotilla-Sanchez [2], Serguei Maximov [1] and Manuel Madrigal-Martínez [1]

[1] Tecnológico Nacional de México, Instituto Tecnológico de Morelia, Av. Tecnológico 1500, Morelia 58120, Michoacán, Mexico; paulinagarcia-pena@hotmail.com (P.G.-P.); serguei.m@morelia.tecnm.mx (S.M.); manuel.mm@morelia.tecnm.mx (M.M.-M.)

[2] School of Electrical Engineering and Computer Science, Oregon State University, Corvallis, OR 97331, USA; ecs@oregonstate.edu

* Correspondence: francisco.rd@morelia.tecnm.mx; Tel.:+52-4432-85-47-15

Abstract

Intentional Controlled Islanding (ICI) is a critical strategy for mitigating cascading failures and preventing large-scale blackouts in power systems. This paper proposes a novel ICI framework based on constrained spectral clustering (CSC), which integrates a data amelioration technique—Hierarchical Amelioration of Clusters (HIAC)—to enhance clustering performance and ensure robust and reliable islanding solutions. The CSC algorithm employs spectral embedding followed by the *k*-medoids clustering method to group coherent generators and partition the system into stable islands. Conventional clustering techniques may produce inconsistent or suboptimal results when applied to systems with overlapping or poorly separated data clusters. The proposed HIAC method addresses this issue by improving cluster compactness and separation. The framework is validated using dynamic simulations of cascading failures on two benchmark systems: the IEEE RTS-96 three-area system and the IEEE 39-bus system. With the RTS-96 test system, due to its modular and symmetric structure, we demonstrate a case with consistent clustering that does not require data amelioration. In contrast, the more intricate topology of the 39-bus system required the HIAC method to obtain a stable islanding configuration. Simulation results confirm that the proposed framework effectively mitigates cascading failures and avoids system-wide blackouts, while reducing load curtailment. The proposed approach enhances the reliability and applicability of ICI under diverse topological conditions.

Keywords: cascading failures; spectral clustering; islanding; power system

Academic Editor: Sergio Cano-Andrade

Received: 2 June 2026
Revised: 8 July 2026
Accepted: 14 July 2026
Published: 15 July 2026

1. Introduction

Although modern power systems are engineered to be robust and resilient against disturbances, their stability can be compromised during severe contingencies, particularly when operating near their dynamic or steady-state limits. Such extreme disturbances may arise from natural hazards (e.g., earthquakes or hurricanes), human operational errors, failures in control systems, hidden faults in protection schemes, or malicious cyber-physical attacks. These initiating events can trigger cascading failures that jeopardise system integrity, potentially resulting in widespread blackouts. As reported in [1], major power outages in 2021 affected over 350 million people—equivalent to more than 4% of the global population—highlighting the growing vulnerability of power grids, as emerging challenges—such as the integration of variable renewable energy sources—compound traditional risks, including extreme weather and ageing infrastructure.

Cascading failures have been a critical factor in major blackouts, such as the North American outage of 14 August 2003 [2]. These failures typically originate from an initiating event, such as a fault or the disconnection of an overloaded transmission line. The initial disturbance can cause propagation through the system by causing further overloads, leading to subsequent outages and a cascade of failures. In addition to line outages, generator oscillations may arise as a consequence of system instability, potentially resulting in out-of-step tripping. Such conditions can escalate further, triggering under-frequency load shedding or additional generator disconnections, thereby exacerbating the severity of the event.

Several studies have demonstrated that many large-scale blackouts—including the 2003 Northeast Blackout [3]—could have been prevented, or their impacts significantly mitigated, had appropriate defensive islanding measures been implemented either prior to or during the disturbance. Defensive islanding, also referred to as intentional controlled islanding (ICI), involves the deliberate partitioning of a power system into smaller, self-sustained islands by disconnecting selected transmission lines. This strategy aims to contain the spread of cascading failures, as the resulting sub-networks are more capable of maintaining local power balance and are less likely to exacerbate instability. Consequently, intentional islanding is regarded as an emergency control action to safeguard the integrity of the power grid under extreme conditions.

The implementation of an effective splitting strategy for intentional islanding involves two principal challenges: (a) determining *where* to island, and (b) identifying *when* to island. In most studies on defensive islanding, it is commonly assumed that separation relays (SRs) are pre-installed at designated separation points and are coordinated at the system level. When islanding is required, only the SRs at selected locations are activated—either simultaneously or in sequence—while others are blocked, thereby forming the desired islands. To address the challenges of spatial and temporal coordination, islanding schemes are typically structured across three time domains: the Offline Analysis (OFA) stage, the Online Monitoring (ONM) stage, and the Real-Time Control (RTC) stage [4]. The question of *where* to island is addressed during the OFA stage, where suitable boundary lines are identified to enable the formation of electrically stable islands. Conversely, the question of *when* to island is resolved in the RTC stage, which determines the appropriate separation time based on real-time synchrophasor measurements (if available) and modal analysis results provided by the ONM stage.

Although extensive research has been conducted on ICI, the two principal challenges—identifying *where* and *when* to separate the network—are often studied independently, despite their strong interdependence. These decisions are closely interrelated in practice, as the spatial partitioning of the grid directly influences the timing and effectiveness of the separation strategy.

To achieve stable islanding, any solution must satisfy a wide range of operational and stability constraints, including load-generation balance, generator coherency, transmission availability, thermal limits, and both voltage and transient stability. Addressing all of these simultaneously is a highly complex and computationally intensive task. Nevertheless, a subset of these constraints—particularly generator coherency and load-generation balance—can serve as a primary basis for defining separation boundaries [5], while the remaining constraints may be managed through secondary corrective measures such as load or generation shedding [6].

Among these constraints, generator coherency is especially critical to the post-separation stability of the formed islands. Severe disturbances in the grid can induce electromechanical oscillations that disrupt synchronism among generators. Those with strong dynamic coupling tend to swing together and are termed *coherent*, whereas those with weak coupling swing against each other [7]. An effective islanding strategy must ensure that coherent generators remain within the same island to preserve transient stability and reduce the risk of further outages. Conversely, assigning non-coherent generators to a single island can lead to rotor angle instability following network separation [8]. Despite this, many existing islanding methods focus solely on identifying optimal separation points without verifying whether the resulting islands maintain dynamic stability or effectively mitigate failure propagation. This shortcoming can result in unbalanced or unstable islands that accelerate the cascading process, potentially propelling the system into a rapid and irreversible blackout phase (i.e., fast cascading phase). Given that ICI is typically deployed as a last line of defence, any failure in its execution may have catastrophic consequences for system integrity.

Recent contributions in the literature have proposed various approaches for implementing ICI, with the objective of partitioning the power system into islands that solely include coherent generators [9–17]. These methods can broadly be classified according to their optimisation goals. Two principal categories emerge: (a) minimisation of power imbalance [9–15], which aims to reduce the mismatch between load and generation within each island; and (b) minimisation of power flow disruption [16,17], which seeks to preserve the original power flow pattern as closely as possible after islanding.

In particular, the latter objective—minimal power flow disruption—can be effectively addressed using advanced graph-theoretic techniques such as *spectral clustering* [18]. This method relies on the eigenvalues and eigenvectors of matrices derived from graphs that encode the system structure. When applied to generator coherency detection, the graph represents the dynamic coupling among generators (a so-called *dynamic graph*) [17]. In the context of partitioning the network, the graph typically represents its topological or weighted structure. Spectral clustering has been employed in several studies [6,7,17,19,20] to derive islanding solutions that minimise disruption to power flows. More broadly, recent reviews have highlighted the increasing role of machine learning and deep learning in coherent power grid partitioning, including data-driven approaches for coherency identification, controlled islanding, and grid partitioning under complex operating conditions [21]. In this context, spectral clustering has also been used as an auxiliary tool in reinforcement-learning-based methods. For example, in [22], a reinforcement learning method is proposed in which spectral clustering is incorporated into a merge-action strategy designed to reshape the action space of the agent, enabling the continuous refinement of current solutions while guaranteeing the *k*-island constraint through a dedicated processing mechanism. Similarly, in [23], a graph-based reinforcement learning model is proposed to design AI-assisted switching strategies in transmission networks, with the objective of mitigating risk by strategically isolating affected areas for self-healing during power outages. In this model, spectral clustering is employed to group similar actions together, thereby addressing the high dimensionality of the action space, accelerating convergence, and supporting the feasibility of the learning process. Finally, in [24], an iterative weight-adjusted constrained spectral clustering (IWCSC) algorithm is developed for a novel risk-triggered preventive islanding method. The IWCSC algorithm is used to generate subgraph partitions that satisfy operational constraints, including generation–load balance, line thermal limits, and voltage magnitude constraints, while minimising disruption to the power flow.

The spectral clustering technique can be viewed as a three-step algorithm [25]. First, a similarity graph is constructed to represent pairwise relationships among data points.

Second, the data are embedded into a lower-dimensional space using the eigenvectors of the graph Laplacian, where cluster structures become more apparent. Finally, a conventional clustering algorithm—such as *k*-medoids—is applied to the embedded data to identify distinct groups.

In studies where spectral clustering has been applied to address the ICI problem, the final step of the algorithm—cluster identification—is typically performed using classic clustering methods such as *k*-means, *k*-medoids, or agglomerative hierarchical clustering (AHC). However, these conventional algorithms exhibit several well-documented limitations that can affect the robustness and accuracy of islanding solutions [26]:

- *k*-means clustering assumes that clusters are spherical and of similar size, which often results in poor performance when applied to datasets with irregularly shaped or imbalanced clusters. Moreover, the algorithm's sensitivity to initial centroid placement can lead to inconsistent outcomes across different runs on the same dataset. Outliers can also distort the centroids, producing skewed or misleading cluster boundaries.
- *k*-medoids, while more robust to outliers than *k*-means, is significantly more computationally intensive, particularly for large datasets. It similarly assumes compact and spherical clusters, and its random initialisation of medoids can yield varied clustering results across different runs.
- The AHC algorithm suffers from the drawback that, once clusters are merged, they cannot be split again, potentially leading to suboptimal solutions. Furthermore, the final clustering is heavily influenced by the choice of linkage criterion (e.g., single, complete, or average), which can introduce structural biases into the resulting partition.

In recent years, researchers have explored various techniques to enhance clustering performance by *ameliorating* the datasets prior to analysis [27–32]. These approaches aim to reshape the data space by introducing artificial gravitational forces between neighbouring points, thereby drawing similar elements closer together. As a result, the modified datasets become more amenable to clustering algorithms, improving the quality of the resulting partitions. Notably, some amelioration methods operate independently of the clustering algorithm itself, enabling a range of clustering techniques to yield more accurate and reliable results when applied to the transformed datasets.

Building upon this premise, the present study proposes a comprehensive framework to be implemented during the OFA stage of ICI, specifically addressing the challenge of determining "where to island" and assessing both the correctness and effectiveness of the ICI operation in suppressing cascading failures. The proposed framework consists of two main components. First, we adopt a graph-theoretic ICI scheme based on constrained spectral clustering (CSC) to identify an islanding solution that minimises power flow disruption while ensuring that each island contains only coherent generators [7]. To improve the clustering performance and overcome the limitations of classic algorithms, an ameliorated-dataset technique is embedded into the scheme [33]. Second, the resulting island configuration is evaluated using an open-access dynamic cascading failure simulation [34], which provides a detailed assessment of the scheme's operational correctness and its effectiveness in suppressing failure propagation.

It is important to emphasise that the objective of this work is not to introduce a completely new islanding paradigm, but to enhance the clustering stage of CSC-based ICI. In particular, the proposed contribution targets the final step of the spectral clustering procedure, where the embedded data are assigned to clusters using a conventional clustering algorithm. Since this step directly determines the resulting island configuration, any limitation of the clustering algorithm may propagate to the final islanding solution. The proposed HIAC procedure is therefore incorporated as a data amelioration stage to improve cluster compactness and separation before the final partition is obtained. In this sense, the novelty of the proposed CSC-HIAC framework lies in improving the robustness and reliability of constrained spectral clustering for ICI, rather than replacing the overall graph-theoretic islanding formulation.

Additionally, the validation stage is another distinguishing aspect of the proposed framework. Many ICI studies assess the quality of the islanding solution mainly through static indicators, such as power imbalance, power flow disruption, or coherency preservation. Although these indicators are essential, they do not fully demonstrate whether the selected islanding action can actually arrest the progression of cascading failures under dynamic operating conditions. In this work, the proposed islanding solution is therefore tested within a dynamic cascading failure simulation environment, allowing its corrective effect to be assessed after network separation. Furthermore, the use of an open-access simulation tool improves transparency and reproducibility, in contrast with studies that rely exclusively on proprietary software for dynamic validation.

In this work, *k*-medoids is adopted in the partitioning stage of both the generator coherency identification and the constrained spectral clustering procedures. This choice is motivated by two main considerations. First, in contrast to *k*-means, which computes virtual centroids that may not correspond to any physical element of the system, *k*-medoids selects actual data points as cluster representatives. In the power system context, this provides a more physically meaningful interpretation, since the medoid can be associated with an existing generator that represents the corresponding coherent group or island. Second, *k*-medoids is more robust than *k*-means in the presence of outliers and transient disturbances, which are expected during cascading events. Nevertheless, *k*-medoids is not free from limitations, since its random initialisation may still lead to inconsistent clustering results when the embedded data are poorly separated. This limitation motivates the integration of the HIAC data amelioration procedure, which improves cluster compactness and separation prior to the final clustering step.

It should also be noted that pure graph-partitioning methods, such as minimum-cut formulations, mainly focus on reducing the disruption associated with the selected cutset. Although this objective is important for preserving the pre-islanding power flow pattern, it does not by itself guarantee that the resulting islands will contain only coherent generators. Therefore, graph partitioning without explicit coherency constraints may lead to dynamically infeasible islanding solutions. This motivates the use of a constrained spectral clustering formulation, in which generator coherency is preserved while the disruption of power flows is minimised.

The contributions of this research are threefold. First, the limitations of classic clustering algorithms in the context of spectral-clustering-based ICI are identified and critically analysed, with particular emphasis on how these limitations may affect the final islanding configuration. Second, rather than proposing a completely new islanding paradigm, this work introduces a targeted enhancement of the constrained spectral clustering framework by integrating the HIAC data amelioration method into its final clustering stage. This improves cluster compactness and separation, leading to more robust and reliable islanding solutions while preserving generator coherency constraints. Third, the proposed scheme is validated using dynamic cascading failure simulations implemented with an open-access tool, thereby assessing not only the correctness of the resulting islanding configuration but also its effectiveness in suppressing failure propagation. This addresses a key limitation in much of the existing literature, where validation is often based on static criteria or conducted using proprietary software, and enhances transparency, reproducibility, and accessibility for further research and practical deployment.

https://doi.org/10.3390/sym18071196

2. Cascading Failure Simulation

Cascading failures in power systems involve a range of complex and nonlinear mechanisms, including voltage collapse, frequency instability, and loss of synchronism. Furthermore, achieving stable islanding requires that the resulting system configuration satisfies a variety of operational and dynamic constraints, such as load-generation balance, generator coherency, thermal limits, transmission availability, and both voltage and transient stability. As such, it is not sufficient to evaluate intentional controlled islanding (ICI) schemes based solely on topological or conventional quasi-steady-state (QSS) models. In this study, to rigorously assess whether the proposed islanding solutions maintain dynamic stability and effectively suppress the propagation of failures, the Cascading Outage Simulator with Multiprocess Integration Capabilities (COSMIC)—originally introduced in [34]—is adopted as a validation tool.

COSMIC is a dynamic, hybrid simulation tool designed to model the intricate interactions between power system dynamics and discrete protection actions during cascading failures. Unlike QSS models, COSMIC captures key nonlinear phenomena—such as voltage collapse, frequency instability, and loss of synchronism—that dominate in the later stages of cascading events. To achieve this, the state of the power system at time t is defined by three vectors:

$\mathbf{x}(t)$: continuous differential state variables (e.g., generator dynamics),

$\mathbf{y}(t)$: continuous algebraic variables (e.g., power flow constraints),

$\mathbf{z}(t)$: discrete state variables (e.g., relay states).

The system is governed by a set of hybrid equations:

$$\frac{d\mathbf{x}}{dt} = \mathbf{f}(t, \mathbf{x}(t), \mathbf{y}(t), \mathbf{z}(t)) \tag{1}$$

$$\mathbf{g}(t, \mathbf{x}(t), \mathbf{y}(t), \mathbf{z}(t)) = 0 \tag{2}$$

$$\mathbf{h}(t, \mathbf{x}(t), \mathbf{y}(t), \mathbf{z}(t)) < 0 \tag{3}$$

The first equation models the dynamic behaviour of synchronous machines and control systems. The second represents the algebraic constraints, including full AC power flow equations. The third describes discrete triggering conditions which, when violated, initiate protection actions that alter the system topology or state.

The core dynamic model includes third-order synchronous machine representations, simplified exciters and governors, and a variety of static and dynamic load models. The differential equations cover generator rotor angle and speed (swing equations), internal voltages, and control mechanisms.

In addition, COSMIC integrates a comprehensive relay protection system, featuring five types of relays: over-current (OC), distance (DIST), temperature-based (TEMP), under-voltage load shedding (UVLS), and under-frequency load shedding (UFLS). Each relay operates with fixed or time-inverse delay logic and triggers appropriate discrete actions when thresholds are violated.

Discrete events—such as relay tripping or system islanding—invoke a re-evaluation of the model. COSMIC uses a recursive event-handling algorithm, and when islanding is detected (via admittance matrix analysis), it solves the differential-algebraic equation (DAE) system separately for each resulting island. Time-domain integration is performed using the trapezoidal method with an adaptive time step, which ensures a balance between numerical accuracy and computational efficiency under both steady-state and transient conditions.

The simulation process is executed through the following main steps (see [34] for detailed implementation):

1. Initialise system model and apply exogenous contingencies.

2. Check for islanding and recursively simulate each island.
3. Integrate the continuous DAE system.
4. Monitor for threshold violations triggering discrete events.
5. Process protection actions and update system state.
6. Continue until steady state or simulation end time is reached.

By incorporating both fast-timescale dynamic behaviour and slower protective mechanisms within a unified framework, COSMIC offers a robust platform for testing the resilience of ICI schemes under realistic conditions. Moreover, its open-access nature promotes transparency, reproducibility, and ease of integration for academic research and development.

3. Intentional Controlled Islanding

This study adopts a controlled islanding approach based on constrained spectral clustering, originally introduced in [7], to determine the optimal partitioning of the power system into stable and coherent islands. The ICI problem is formulated as a constrained optimisation task, which is then transformed into a graph *min-cut* problem to facilitate efficient identification of separation boundaries. The methodology is developed through four components: the graph-based modelling of the power grid, the definition of generator coherency constraints, the construction of a constraint matrix, and the application of constrained spectral clustering to minimise power flow disruption while preserving dynamic stability.

3.1. Power Grid as a Graph

A power grid can be represented as a weighted, undirected graph $G(N, E)$ where N denotes the set of nodes (buses) and E represents the set of edges (transmission lines or transformers). To account for the system's operating condition, the edge weights are determined using the average of the absolute values of the active power flows in both directions:

$$\mathbf{W} = \begin{cases} w_{ij} = \frac{|P_{ij}| + |P_{ji}|}{2} & i \neq j \\ w_{ij} = 0 & i = j \end{cases}. \tag{4}$$

Spectral clustering is based on the use of graph Laplacian matrices, which encode the structural and weight information of the graph. Two common variants are the unnormalised Laplacian and the normalised Laplacian. The unnormalised Laplacian matrix $\mathbf{L}$ is defined as:

$$\mathbf{L} = \begin{cases} -w_{ij} & i \neq j \\ d_{ii} & i = j' \end{cases} \tag{5}$$

where the diagonal element d_{ii} is the sum of the weights of all edges incident to node i:

$$d_{ii} = \sum_{j=1}^{N} w_{ij}. \tag{6}$$

The unnormalised Laplacian can also be written compactly as $\mathbf{L} = \mathbf{D} - \mathbf{W}$, where $\mathbf{D}$ is the diagonal degree matrix with entries d_{ii}, and $\mathbf{W}$ is the weighted adjacency matrix. The normalised Laplacian $\mathbf{L}_n$ is then defined as:

$$\mathbf{L}_n = \mathbf{D}^{-1/2}\mathbf{L}\mathbf{D}^{-1/2}. \tag{7}$$

This matrix formulation provides the foundation for applying spectral clustering techniques, which use the eigenstructure of the Laplacian to identify optimal graph partitions.

https://doi.org/10.3390/sym18071196

3.2. Generator Grouping Constraints

To enhance transient stability and reduce the risk of further outages, an islanding solution must be constructed such that coherent generators are assigned to the same island. In the system under consideration, coherent generator groups are identified by constructing a dynamic graph, in which nodes represent generators and edge weights correspond to their dynamic coupling—quantified by the synchronising torque coefficients. Normalised spectral clustering is then applied to this dynamic graph to cluster generators based on their coupling strength.

Using the Laplacian matrix of the dynamic graph, the following linearised second-order dynamic model of a system with g generators is adopted:

$$\Delta\ddot{\boldsymbol{\delta}} = \mathbf{M}^{-1}\mathbf{K}\Delta\boldsymbol{\delta}, \tag{8}$$

where $\Delta\boldsymbol{\delta}$ denotes the vector of generator rotor angle deviations, and $\mathbf{M}$ and $\mathbf{K}$ are the generator inertia matrix and synchronising torque coefficient matrix, respectively.

To determine coherent generator groups, the algorithm introduced in [8] is applied as follows:

1. Input the number of generators r and the desired number of clusters k.
2. Compute the first k eigenvalues and corresponding eigenvectors of the matrix $\mathbf{M}^{-1}\mathbf{K}$, sorted in increasing order of eigenvalue magnitude.
3. Discard the first eigenvector, and normalise the remaining $k-1$ eigenvectors to have unit Euclidean norm.
4. Form the matrix $\mathbf{X}^{r\times k}$ by combining the normalised eigenvectors, and apply the k-medoids algorithm to group the rows of $\mathbf{X}$ into k clusters.
5. Output the resulting clustering, which defines the generator assignments to coherent groups.

These generator grouping constraints will later be integrated into the spectral clustering formulation to ensure that coherent generators remain within the same island.

3.3. Constraint Matrix

To ensure that coherent generators remain within the same island during clustering, a constraint matrix $\mathbf{Q}$ is constructed. This matrix encodes two types of pairwise constraints between nodes:

- Must-Link (ML) constraints, which require that two nodes must belong to the same cluster, and
- Cannot-Link (CL) constraints, which prohibit two nodes from being assigned to the same cluster.

The matrix $\mathbf{Q} \in \mathbb{R}^{N\times N}$ is defined element-wise as:

$$Q_{ij} = Q_{ji} = \begin{cases} +1, & if\ (i,j)\mathrm{ML} \\ -1, & if\ (i,j)\mathrm{CL}\,. \\ 0, & Otherwise \end{cases} \tag{9}$$

This matrix is then normalised to obtain $\mathbf{Q}_n$, which aligns with the structure of the normalised graph Laplacian used in spectral clustering. The normalisation is defined as:

$$\mathbf{Q}_n = \mathbf{D}^{-1/2}\mathbf{Q}\mathbf{D}^{-1/2}. \tag{10}$$

The normalised constraint matrix $\mathbf{Q}_n$ is incorporated into the spectral clustering framework to guide the partitioning process, ensuring that dynamic coherency constraints among generators are respected.

https://doi.org/10.3390/sym18071196

3.4. Minimising the Power-Flow Disruption While Preserving Coherent Generator Groups

To determine an islanding solution that minimises power flow disruption while satisfying the generator coherency constraint, the method adopted in this study solves a normalised min-cut problem on graph G using constrained spectral clustering in a relaxed optimisation form. The objective function is expressed as:

$$argmin\ \mathbf{v}^T \mathbf{L}_n \mathbf{v}, \tag{11}$$

subject to the following constraints:

$$\mathbf{v}^T \mathbf{Q}_n \mathbf{v} \ \geq \beta, \tag{12}$$

$$\mathbf{v}^T \mathbf{v} = vol = \ \sum_{i=1}^{N} d_{ii}, \tag{13}$$

$$\mathbf{v} \ \neq \ \mathbf{D}^{1/2} 1_N^T. \tag{14}$$

Here, $\mathbf{v}$ is the eigenvector of the normalised Laplacian matrix, *vol* is the volume of the graph G, defined as the sum of the degrees of all nodes, β is a threshold parameter ensuring constraint satisfaction, and $\mathbf{1}_N^T$ is the all-ones vector of size N.

As shown in [35], the optimal solution to the constrained minimisation problem in (11)–(14) can be obtained by solving the following generalised eigenvalue problem:

$$\mathbf{L}_n \mathbf{v} = \ \lambda \left(\mathbf{Q}_n - \frac{\beta}{vol} \mathbf{I} \right) \mathbf{v}. \tag{15}$$

The constrained spectral clustering algorithm proceeds through the following steps:

1. Define the number of clusters k based on generator coherency information.
2. Compute the edge weight matrix using (4), as well as the degree matrix $\mathbf{D}$ and graph volume *vol*.
3. Construct the normalised Laplacian matrix $\mathbf{L}_n$ using Equations (5) and (7).
4. Form the normalised constraint matrix $\mathbf{Q}_n$ using generator coherency data.
5. Solve the generalised eigenvalue system defined in (15).
6. Discard eigenvectors associated with zero or negative eigenvalues.
7. Normalise the remaining eigenvectors using:

$$\mathbf{v} \ \leftarrow \ \frac{\mathbf{v}}{\|\mathbf{v}\|} \sqrt{vol}.$$

8. Select the $k-1$ eigenvectors corresponding to the smallest $k-1$ positive eigenvalues.
9. Form the matrix $\mathbf{V}^* \leftarrow argmin\ \mathbf{V}^T L_n \mathbf{V}$, where $\mathbf{V} \in \mathbb{R}^{N\times(k-1)}$ contains the selected eigenvectors as columns.
10. Cluster the nodes using the k-medoids algorithm applied to the rows of $\mathbf{V}^*$.

This procedure yields an islanding configuration that not only minimises the disturbance to power flows but also preserves dynamic coherency among generators—two essential conditions for preventing further instability following system separation.

It should be noted that the coherency analysis based on Equation (8) relies on a linearised second-order electromechanical model around a given operating point. This model is widely used for identifying generator groups that tend to swing together, since the eigenvectors of $\mathbf{M}^{-1}\mathbf{K}$ associated with the smallest eigenvalues provide useful information about slow electromechanical modes and coherent generator behaviour. However, the model remains an approximation and may not fully capture severe nonlinear transient phenomena, such as large rotor-angle excursions, nonlinear excitation and governor responses, protection-triggered topology changes, converter-interfaced generation dynamics, or disturbance-dependent coherency variations. Therefore, the resulting generator groups are interpreted in this work as offline coherency constraints for the CSC-based islanding procedure, rather than as a complete nonlinear transient coherency assessment.

A full time-domain coherency evaluation is not included in this study because the main objective is to enhance the constrained spectral clustering stage used to determine islanding boundaries. Time-domain coherency identification would require extensive nonlinear dynamic simulations across multiple contingencies, operating points, and clearing times, and may produce scenario-dependent coherency groupings. Instead, the present framework uses the linearised coherency model to define generator grouping constraints during the Offline Analysis stage, and subsequently evaluates the resulting islanding solutions through dynamic cascading failure simulations. Future work will consider PMU-based and time-domain coherency assessment to update generator groups under severe nonlinear and renewable-rich operating conditions.

4. Improving the Accuracy of Clustering Algorithms

While the previous section outlined a constrained spectral clustering approach for identifying optimal islands, the accuracy and robustness of the final islanding solution are strongly influenced by the performance of the clustering algorithm applied in the final step. Conventional clustering algorithms often struggle when applied to power system datasets with overlapping cluster structures or ambiguous boundaries. Moreover, as discussed in the Section 1, classic algorithms such as *k*-means, *k*-medoids, and agglomerative hierarchical clustering exhibit several limitations that can adversely affect clustering outcomes. To address these challenges and improve the reliability of the islanding process, this section presents a data preprocessing strategy aimed at enhancing the structure of the dataset prior to clustering.

Clustering algorithms are central to various intentional controlled islanding (ICI) methods that rely on spectral techniques. These algorithms uncover the underlying structure of data by grouping elements based on their similarities. In general, there are datasets—referred to as *good* datasets—on which most clustering algorithms perform well, due to a clear separation between data clusters. In these cases, the inter-cluster distance is significantly greater than the intra-cluster distance, allowing the clusters to be easily identified. Conversely, *bad* datasets are characterised by overlapping cluster boundaries and similar inter- and intra-cluster distances, making it difficult for clustering algorithms to achieve accurate results.

To improve the performance of clustering algorithms on such challenging datasets, it is essential to increase the contrast between inter- and intra-cluster distances. In this context, Ref. [33] proposes an innovative data preprocessing method known as the HIAC algorithm (High-Intensity Attraction Clustering), which is designed to enhance the structural characteristics of the data before clustering. The fundamental idea behind HIAC is to use a gravity-based model to shift similar data points closer together (referred to as object motion), thereby increasing intra-cluster cohesion while separating dissimilar groups. In addition, HIAC classifies neighbouring points into valid neighbours (high similarity) and invalid neighbours (low similarity), and it locks the original neighbour relationships during the object motion process to preserve topological consistency before and after the process.

The HIAC algorithm comprises the following three steps:

1. **Construction of a topology graph**, representing the dataset's structure.
2. **Identification of valid neighbours**, based on similarity thresholds.
3. **Object motion**, which iteratively modifies the data distribution to amplify cluster distinctiveness.

4.1. Constructing the Topology Graph for the Dataset

In the first step of the HIAC algorithm, a topology graph is constructed to represent the structural relationships within the dataset. In this graph, each data object is treated as a vertex, and connections are formed between each vertex and its x-nearest neighbours, where x is a user-defined input parameter. These connections define the edges of the graph, which are weighted based on pairwise distances between objects.

The weight of the edge between two objects o_i and o_j, denoted by w_{ij}, is defined as

$$w_{ij} = -\left\|o_i - o_j\right\|_2 + \max_{o_p, o_q \in O}\left\|o_q - o_p\right\|_2, \tag{16}$$

where O is the dataset to be analysed, $\|\cdot\|_2$ denotes the Euclidean norm (2-norm), and the term $\max_{o_p, o_q \in O}\left\|o_q - o_p\right\|_2$ ensures that all edge weights remain non-negative by shifting the distance range.

This formulation guarantees that objects that are closer in Euclidean space are connected with larger edge weights, while those that are further apart are assigned smaller weights. The resulting graph provides a structured representation of local object similarity, which serves as the basis for the subsequent steps of the HIAC algorithm.

4.2. Identifying Valid-Neighbours

Rather than identifying valid neighbours directly, the HIAC algorithm adopts a novel strategy by first identifying and eliminating invalid edges—i.e., those that link invalid neighbours. This is achieved through a probabilistic analysis of edge weights derived from the topology graph constructed in the previous step.

To begin, the set of all edge weights is partitioned into equal-length intervals. The length of each interval is defined as:

$$dc = 10 \times \frac{(max(W) - min(W))}{No}, \tag{17}$$

where No is the number of objects in the dataset O, and W_i represents the object weight of object o_i, calculated as

$$W_i = \frac{1}{\mathrm{x}} \sum_{j \in \emptyset(o_i)} w_{ij}, \tag{18}$$

where $\emptyset(o_i)$ denotes the set of x-nearest neighbours of object o_i.

The HIAC algorithm then constructs a probability decision graph by estimating the empirical distribution of object weights across the defined intervals. The probability associated with the g-th interval is computed as:

$$P(min(W) + g \times dc) = \frac{\sum_{j=1}^{N} \varphi_g(W_j)}{No}, \tag{19}$$

where the indicator function $\varphi_g(W_j)$ is defined as:

$$\varphi_g(W_j) = \begin{cases} 1, if\ min(W) + (g-1) \times dc \le W_j < min(W) + g \times dc \\ 0, otherwise \end{cases}. \tag{20}$$

This process yields a probabilistic profile of edge weight distributions, enabling the algorithm to distinguish between edges that are structurally significant and those that are likely to reflect weak or noisy relationships.

Finally, an observational method is employed to determine a threshold for separating effective from ineffective edges within the decision graph. Edges with weights falling below this threshold are classified as invalid and are consequently pruned from the topology graph. This pruning step sharpens the structural clarity of the data and enhances the clustering process in the subsequent stage.

https://doi.org/10.3390/sym18071196

4.3. Object Motion

In the final step of the HIAC algorithm, object motion is applied to reshape the dataset and enhance cluster separability. For each object connected by an effective edge (as identified in the previous step), the algorithm simulates motion by applying Newton's law of universal gravitation. In this formulation, each object is treated as a vector, allowing the gravitational influence to be directional.

The updated position of object o_i, denoted as $\overrightarrow{o_i'}$, is given by:

$$\overrightarrow{o_i'} = \overrightarrow{o_i} + T \sum_{l=1}^{d} G^l \sum_{j=1}^{s} \frac{\left\| \overrightarrow{o_i^*} - \overrightarrow{o_i^l} \right\|_2 \left(\overrightarrow{o_{ij}} - \overrightarrow{o_i^l} \right)}{\left\| \overrightarrow{o_{ij}} - \overrightarrow{o_i^l} \right\|_2^2}, \tag{21}$$

where

$\overrightarrow{o_i}$ is the vector form of o_i,

$\overrightarrow{o_{ij}}$ is the j-th valid-neighbour of $\overrightarrow{o_i}$,

s is the number of valid neighbours,

d is the number of time-segments,

t is the duration of each time-segment, and $T = \frac{1}{2}t^2$ is a scaling factor,

$\overrightarrow{o_i^l}$ is the vector of o_i in the l-th time segment,

$\overrightarrow{o_i^*}$ is the nearest valid-neighbour of o_i,

$G^l = \frac{1}{No} \sum_j^{No} \left\| \overrightarrow{o_j^*} - \overrightarrow{o_j} \right\|_2$ is the gravitational constant in the l-th time segment, and

No is the total number of objects in the dataset.

The purpose of this motion is to bring similar objects closer together while maintaining structural constraints imposed by the valid-neighbour relationships. Over multiple iterations, this process enhances the compactness of clusters and increases inter-cluster separation, thereby transforming the dataset into a more suitable form for clustering. The two parameters introduced in this step—T and d—are user-defined and control the extent and duration of object motion, respectively.

Computational Complexity Analysis

The proposed CSC-HIAC framework is intended to be implemented during the Offline Analysis (OFA) stage of ICI, where the question of where to island is addressed by identifying suitable separation boundaries in advance. Therefore, the method is not subject to the same strict execution-time constraints as real-time control actions associated with the decision of when to island. Nevertheless, computational scalability is an important consideration for practical applications.

The computational complexity of the CSC-based ICI stage is dominated by three main operations. Let N denote the number of buses, E the number of transmission lines, k the targeted number of islands, and I the number of clustering iterations. First, constructing the network adjacency matrix, weighted by active or apparent power flow, and incorporating generator coherency constraints through pairwise must-link and cannot-link relations requires $O(N^2)$ operations. Second, projecting the graph Laplacian into the feasible constraint subspace and extracting the first k eigenvectors require $O(N^3)$ operations. Third, clustering the N low-dimensional coordinate rows into k island zones requires $O(IkN^2)$ operations. Thus, the overall time complexity of the CSC-based ICI stage can be expressed as: $O(N^2) + O(N^3) + O(IkN^2)$.

For the HIAC stage, the computational burden is associated with valid-neighbour identification and object movement. In the valid-neighbour identification stage, HIAC computes the weights between each object and its x neighbours, resulting in a complexity of $O(xN)$. In the object movement stage, HIAC computes gravitational values between objects and their valid neighbours over d iterations, resulting in a complexity of $O(dsN)$, where s is the average number of valid neighbours and $s < x$. Therefore, the total complexity of HIAC is: $O(xN + dsN)$.

Consequently, the additional computational cost introduced by HIAC is lower than the dominant eigen-decomposition cost of the CSC procedure for fixed x, d, and s. The proposed CSC-HIAC framework therefore improves the robustness of the final clustering stage without changing the dominant complexity order of the overall CSC-based islanding scheme.

5. Cases Studies

To evaluate the effectiveness of the proposed intentional controlled islanding (ICI) framework, two benchmark power systems are considered: the IEEE RTS-96 three-area system and the IEEE 39-bus system. These systems serve complementary roles in the assessment: one illustrates a case where clustering performs reliably without the need for enhancement, and the other demonstrates the advantages of applying the proposed data amelioration method to address the limitations of classic clustering algorithms.

The analysis begins with the IEEE RTS-96 three-area system, a structurally balanced, multi-area power system composed of three identical subsystems, each with equivalent topology, generation capacity, and load (2850 MW). The system consists of 73 buses and 120 branches, with a total load of 8550 MW. In this analysis, the objective is to partition the system into three islands—corresponding to its predefined areas—with no loss of generality. Because each subsystem is largely self-sufficient and loosely interconnected, the expected islands align naturally with the system's internal structure, allowing for a straightforward validation of the constrained spectral clustering (CSC) method. In this case, the k-medoids algorithm alone is sufficient to obtain accurate and stable clustering results, as the data clusters are well separated. Therefore, this case exemplifies a scenario where classic clustering techniques work effectively without requiring data preprocessing or enhancement.

The second part of the analysis focuses on the IEEE 39-bus system, which represents a snapshot of the New England 345 kV transmission network with 10 generators and 46 branches. In contrast to the RTS-96 system, the IEEE 39-bus network features a more complex and less modular topology, making the identification of coherent and operationally viable islands significantly more challenging. Here, direct application of clustering algorithms yields inconsistent results due to overlapping or poorly separated data clusters. Consequently, to improve clustering performance and solution reliability, we apply the proposed HIAC data amelioration technique in conjunction with the CSC algorithm.

In both systems, cascading failures triggered by line outages are simulated using the COSMIC simulator to validate the ability of the proposed ICI framework to mitigate the propagation of failures and prevent system-wide blackouts. Also, in both systems voltage magnitudes at all buses were chosen as the primary metric to monitor the dynamic evolution of cascading failures. Voltage behaviour provides a direct, system-wide indicator of stability and operational integrity, capturing key phenomena such as voltage sags, instability onset, relay-triggered disconnections, and cascade progression. Unlike power flow or frequency metrics, which may remain relatively stable until critical thresholds are crossed, voltage deviations typically offer early insight into cascading propagation and the system's ability—or inability—to reach a new steady state. Therefore, voltage magnitudes serve as a comprehensive and sensitive proxy to evaluate the effectiveness of islanding solutions during failure scenarios where dynamic mechanisms are involved.

5.1. Baseline Cascading Failure Scenarios in the IEEE RTS-96 Three-Area System

The first case study focuses on the IEEE RTS-96 three-area system. Two baseline cascading failure scenarios are simulated using the open-access COSMIC dynamic simulator to assess the system's vulnerability under severe contingencies in the absence of islanding actions. The simulation end-time for each scenario is set to 300 s to capture the entire evolution of cascading failure events, including the dynamic response of the system and the onset of instability or blackout.

In the first scenario, the initiating event is the simultaneous tripping of transmission lines 66 (215–221), 67 (215–221), 73 (218–221), and 74 (218–221) at $t = 10$ s, representing the automatic isolation of a severe fault by the protection system. Voltage magnitudes at all buses are continuously monitored to observe the progression of instability. As shown in Figure 1, the system experiences significant voltage disturbances following the initial event. At $t = 11.17$ s, a distance relay trips branch 72, further weakening the network. Despite initial attempts at stabilisation, the situation deteriorates, and at $t = 47.37$ s, the simulation fails to converge to a valid operating point. The system is thus declared to have entered a blackout state, with the entire load of 8550 MW lost.

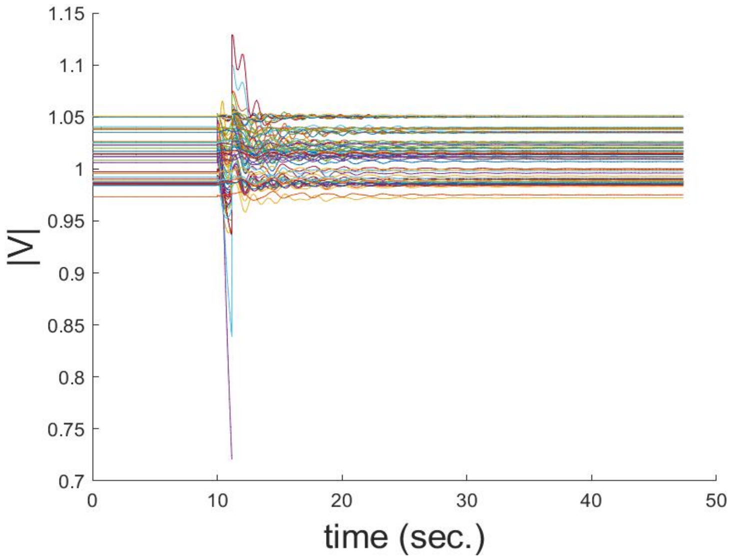

Figure 1. Bus voltage magnitudes over time following the trip of lines 66, 67, 73, and 74 at $t = 10$ s in the IEEE RTS-96 three-area system. Each trajectory corresponds to one bus voltage magnitude. The system enters a blackout state at $t = 47.37$ s following a set of subsequent relay operations.

In the second scenario, a different contingency is introduced by tripping transmission lines 100 (312–323), 101 (313–323), and 120 (323–325) at $t = 10$ s. The voltage dynamics are illustrated in Figure 2. At $t = 11.025$ s, an under-voltage load shedding (UVLS) relay activates at Bus 314, resulting in the disconnection of 48.50 MW of load. Shortly after, at $t = 11.05$ s, another UVLS relay trips at Bus 303, shedding an additional 45.00 MW. Despite these remedial actions, instability continues to propagate. At $t = 84.09$ s, an overcurrent relay trips Branch 102, aggravating the system condition. Finally, at $t = 84.67$ s, the simulation again fails to reach a stable solution, and a full system blackout is declared, with the entire system load lost.

These baseline cases provide a benchmark for comparison against the islanding strategies evaluated in the following subsections, enabling a clear assessment of the extent to which the proposed framework can mitigate cascading events and prevent total blackout.

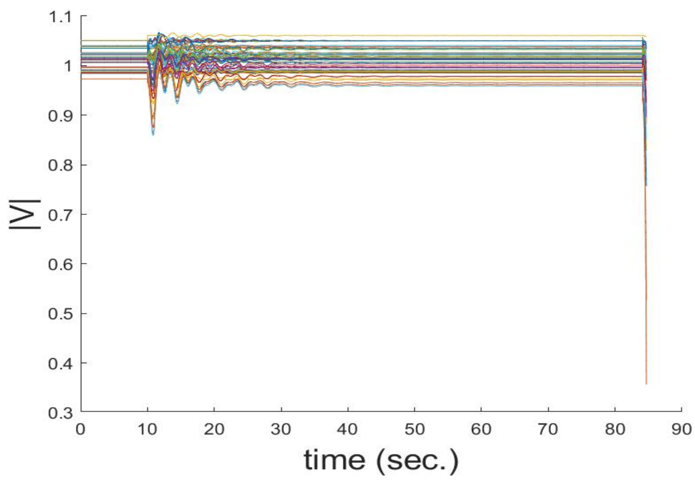

Figure 2. Bus voltage magnitudes over time following the trip of lines 100, 101, and 120 at $t = 10$ s in the IEEE RTS-96 three-area system. Despite UVLS actions, the system collapses at $t = 84.67$ s, resulting in a total blackout.

5.2. Clustering and Islanding Results for the IEEE RTS-96 Three-Area System

In this study, we apply the ICI framework to the IEEE RTS-96 system with the objective of partitioning the network into three stable islands. With no loss of generality, this number of islands was selected to match the system's inherent three-area structure and to assess the effectiveness of the CSC method under favourable clustering conditions. The ICI framework is based on the constrained spectral clustering (CSC) algorithm, as described in Section 3, which integrates coherency constraints and minimises power flow disruption. The final grouping of generators and buses into islands is achieved using the *k*-medoids clustering algorithm.

To assess the robustness and consistency of the clustering outcomes, the CSC algorithm was executed 100 times. Across all runs, the algorithm consistently identified the same coherent generator groups and the same groupings of nodes into islands, demonstrating the stability and reliability of the clustering process. As a result, the HIAC data amelioration method introduced in Section 4 was not necessary for this test case.

Figure 3 shows the islanding solution obtained using the CSC algorithm. As expected, each identified island corresponds closely to one of the three predefined areas in the RTS-96 system. This alignment demonstrates that the CSC algorithm is effective in systems with clear structural separations and can successfully identify meaningful island boundaries that preserve generator coherency and local self-sufficiency.

Figure 4 illustrates the spectral embedding of the RTS-96 system in $\mathbb{R}^2$, obtained without the application of the HIAC data amelioration method. This embedding is based on selecting r eigenvectors of the normalised Laplacian $\mathbf{L}_n$, which project the nodes (buses) into a Euclidean space $\mathbb{R}^r$. In this transformed space, each node is treated as a data point for clustering via *k*-medoids. As can be seen in this figure, the data points are clearly grouped and well separated, with no overlapping boundaries and sufficiently large inter-cluster distances. This visual confirmation explains why the *k*-medoids algorithm performed reliably without further enhancement. In Figure 4, square markers are used to represent the nodes of each island, coloured consistently with the corresponding islands shown in the system diagram in Figure 3, where islands are enclosed by coloured contours.

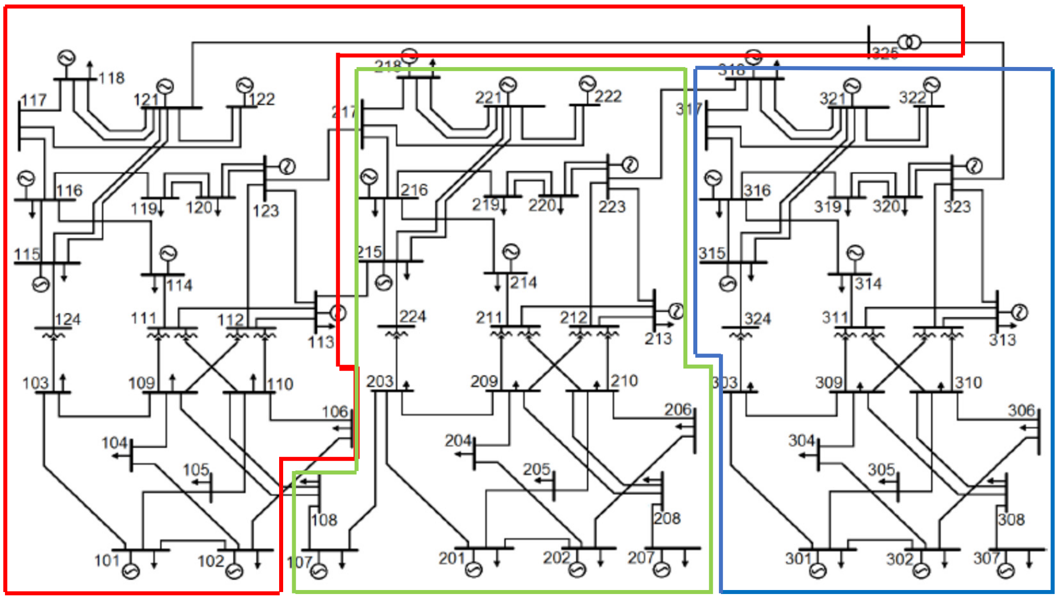

Figure 3. Islanding solution for the IEEE RTS-96 3-area system obtained using the CSC algorithm. The coloured contours indicate the island boundaries: the red contour corresponds to Island 1, the green contour corresponds to Island 2, and the blue contour corresponds to Island 3. The cut-set transmission lines are the inter-area branches crossing the coloured island boundaries. The resulting solution corresponds to the three predefined areas, confirming the effectiveness of the clustering process.

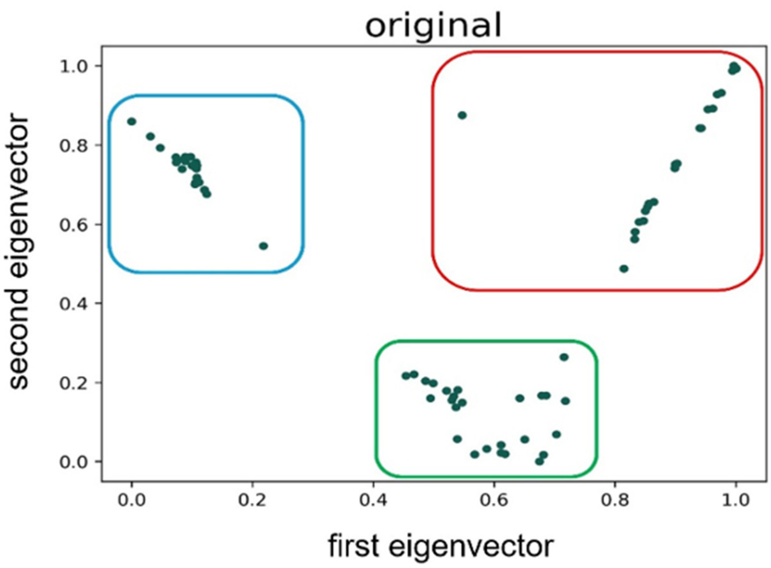

Figure 4. Spectral embedding of the RTS-96 system in $\mathbb{R}^2$ without data amelioration. Square markers indicate the nodes belonging to each island, coloured consistently with Figure 3. The well-separated clusters with no overlapping boundaries demonstrate that the *k*-medoids algorithm performs reliably under favourable data conditions.

5.3. Evaluation of the Islanding Solution for Mitigation of Cascading Failures for the IEEE RTS-96 Three-Area System

The effectiveness of the identified islanding solution was evaluated under the first cascading failure scenario, which is initiated by the tripping of lines 66 (215–221), 67 (215–221), 73 (218–221), and 74 (218–221) at $t = 10$ s. Dynamic simulations were performed using the COSMIC simulator to assess the system's response following the application of the islanding action. The resulting voltage trajectories of the buses are illustrated in Figure 5.

As shown in the figure, the proposed islanding strategy successfully mitigates the cascading failure and averts a system-wide blackout. Despite the need for some load shedding during the intentional separation, the post-islanding configuration maintains dynamic stability across the three islands. The total load shed as a result of the islanding action is approximately 3146 MW, representing a substantial reduction but preserving more than half of the system's total demand. Nevertheless, the islands remain operational, validating the capability of the proposed method to preserve partial service and avoid a complete blackout, while priming the system to perform faster restoration of the load that was shed as a protection mechanism.

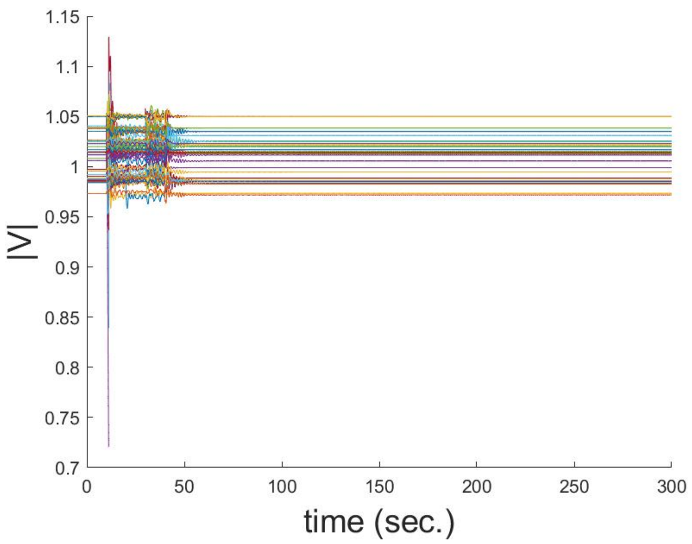

Figure 5. Dynamic simulation results of islanding action applied for the fault scenario initiated by the tripping of lines 66, 67, 73, and 74 at $t = 10$ s in the IEEE RTS-96 three-area system. The voltage trajectories demonstrate that the obtained islanding solution mitigates the cascading failure and prevents a total system blackout, with a total load shedding of approximately 3146 MW.

The islanding solution was also evaluated under the second cascading failure scenario, which is initiated by the tripping of lines 100 (312–323), 101 (313–323), and 120 (323–325) at $t = 10$ s. The dynamic simulation was again conducted using the COSMIC simulator, and the resulting voltage trajectories of all buses are presented in Figure 6. As illustrated in the figure, the proposed islanding scheme successfully mitigates the propagation of the cascading failure, preventing a total system blackout. Although load shedding is required during the intentional separation process, the system remains dynamically stable across all islands. The total amount of load shed in this case is approximately 2850 MW, demonstrating the effectiveness of the proposed strategy in preserving a significant portion of the system load while ensuring operational continuity.

The IEEE RTS-96 3-area system validated the effectiveness of the proposed CSC-based ICI framework under favourable clustering conditions. The algorithm consistently identified stable islands aligned with the system's natural structure, requiring no data amelioration. Moreover, the islanding actions successfully mitigated cascading failures and prevented total blackouts, demonstrating the framework's robustness and practical value to perform timely restoration functions.

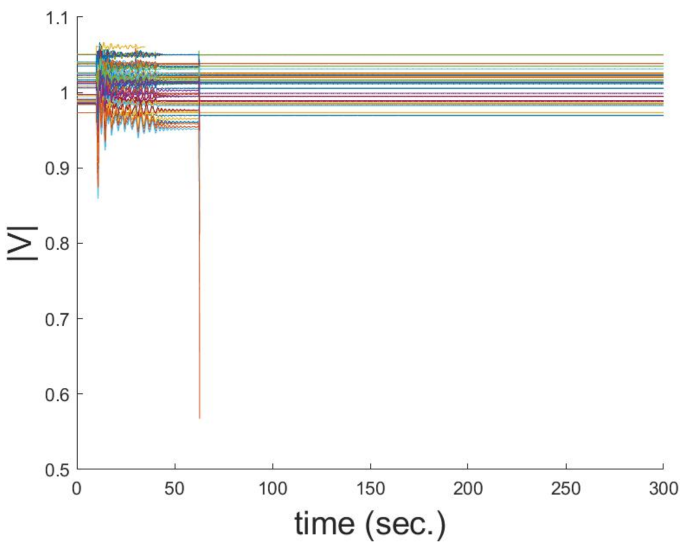

Figure 6. Dynamic simulation results of islanding action applied for the fault scenario initiated by the tripping of lines 100, 101, and 120 at $t = 10$ s in the IEEE RTS-96 three-area system. The voltage trajectories demonstrate that the obtained islanding solution mitigates the cascading failure, preserving system stability with a total load shedding of approximately 2850 MW.

5.4. Baseline Cascading Failure Scenarios in the IEEE 39-Bus System

To further validate the proposed ICI framework under more complex and less structured network conditions, cascading failure scenarios are simulated on the IEEE 39-bus system using the COSMIC dynamic simulator. This test system presents a more challenging environment for islanding due to its less pronounced modularity and more irregular topology. As a baseline for comparison, two distinct cascading failure scenarios are considered. In the first case, the trip of Line 18 (13–14) is simulated at $t = 10$ s. In the second case, Line 31 (26–27) is tripped at the same simulation time. For both scenarios, the total simulation time is set to 300 s to capture the full progression of cascading events, system dynamics, and potential blackout onset.

Figure 7 shows the voltage trajectories of all buses in the case of the Line 18 trip. A clear collapse in voltage profiles is observed as the cascade unfolds. The first line trip occurs at $t = 10$ s, representing the disconnection of Line 18 due to a severe fault. Following this initial event, the system exhibits sustained and growing electromechanical oscillations, indicating a state of dynamic instability. At approximately $t = 37.29$ s, an overcurrent relay trips Line 12, further aggravating the disturbance. Subsequently, at around $t = 90$ s, the under-voltage load shedding scheme begins to operate, disconnecting loads at buses 4, 7, 8, 15, 16, 18, 20, 21, and 24. However, rather than stabilising the system, these actions amplify the oscillatory behaviour. Finally, at $t = 98.3$ s, the simulation fails to converge to a feasible operating point, and the system is declared to have entered a blackout state.

Figure 8 presents the analogous results for the Line 31 case, again demonstrating system-wide instability leading to a complete blackout. In this case, the initial line trip also occurs at $t = 10$ s, corresponding to the disconnection of Line 31. As the disturbance propagates through the system, an overcurrent relay trips Line 3 at approximately $t = 68.83$ s. However, at this same instant, the simulation is unable to converge to a valid operating point, and the system is consequently declared to be in a state of total blackout.

These scenarios form the basis for evaluating whether the ICI framework can effectively mitigate the cascading process and prevent blackout.

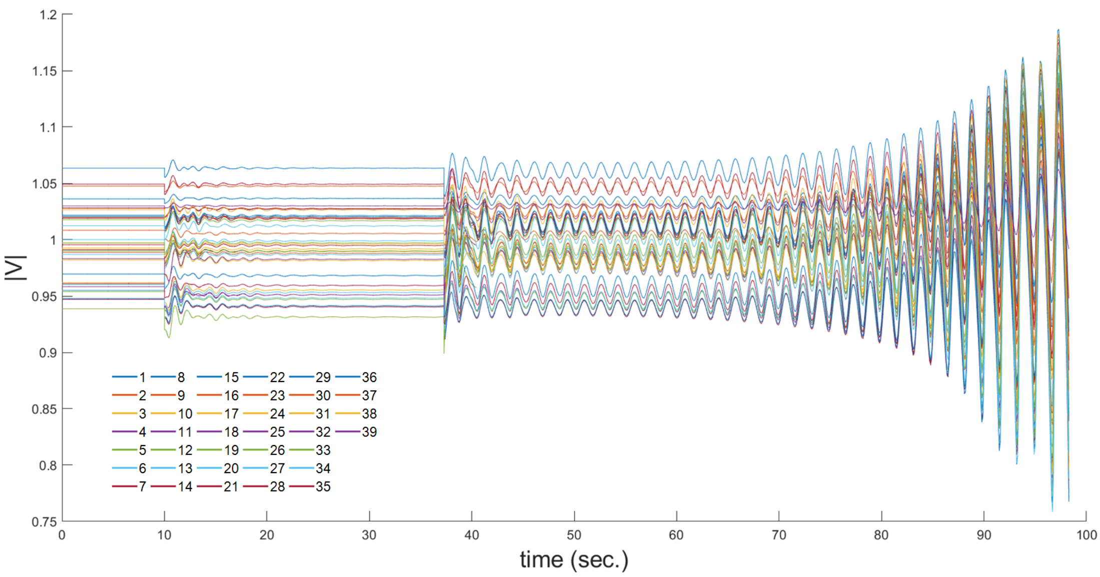

Figure 7. Bus voltage magnitudes over time following the trip of Line 18 at $t = 10$ s in the IEEE 39-bus system. The system exhibits growing oscillations and fails to stabilise, leading to widespread load shedding and ultimately a total blackout at $t = 98.3$ s.

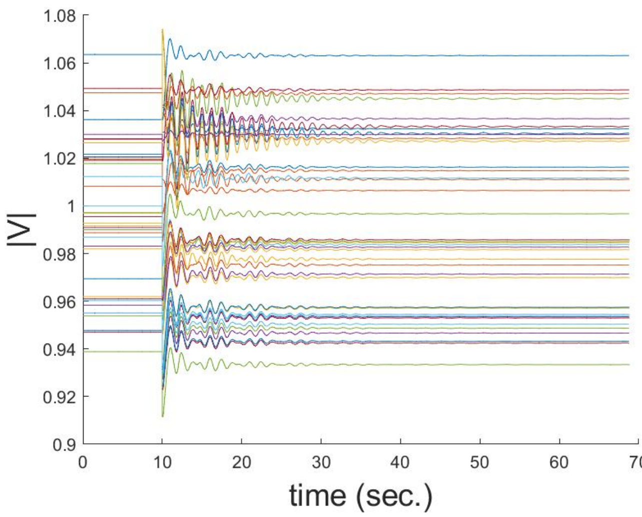

Figure 8. Bus voltage magnitudes over time following the trip of Line 31 at $t = 10$ s in the IEEE 39-bus system. The system experiences severe instability, and a total blackout is declared at $t = 68.83$ s when the simulation fails to converge.

5.5. Clustering and Islanding Results for the IEEE 39-Bus System

In this part of the study, we apply the ICI framework to the IEEE 39-bus system with the objective of partitioning the network into three stable islands. It should be noted that the number of groups k is specified as an input to the generator grouping algorithm; the algorithm then assigns the generators to the k groups rather than determining the optimal value of k automatically. In this study, $k = 3$ was selected as the target number of coherent generator groups/islands for the IEEE 39-bus system. The resulting coherent generator groups are Group 1 = {39}; Group 2 = {30, 31, 32, 37, 38}; and Group 3 = {33, 34, 35, 36}. These groups are used as coherency constraints in the CSC-based islanding procedure to ensure that generators belonging to the same coherent group remain in the same island.

The final grouping of generators and buses into islands is also achieved using the k-medoids clustering algorithm in the CSC-based islanding procedure. However, it is well known that the k-medoids algorithm relies on a random initialisation of medoids, which may lead to different clustering outcomes across different executions. To assess this variability, the CSC algorithm was executed 100 times, resulting in three distinct islanding solutions, which are illustrated in Figure 9.

To address this sensitivity and improve the robustness and consistency of the islanding results, we propose to incorporate the ameliorated-dataset technique known as HIAC, introduced in [29] and detailed in Section 4. The HIAC algorithm is applied to enhance the geometric separation and compactness of the data clusters prior to clustering, thereby enabling the CSC algorithm to consistently identify the optimal islanding configuration. In particular, HIAC is applied to the dataset generated in Step 9 of the CSC algorithm (see Section 3.4), where the spectral embedding of graph G is constructed.

Figure 10a displays the spectral embedding of the IEEE 39-bus system in $\mathbb{R}^2$, prior to data amelioration. It can be observed that the clusters are poorly separated, with overlapping boundaries and limited inter-cluster spacing. After applying the HIAC algorithm to this data, the ameliorated embedding is shown in Figure 10b, where the cluster compactness is significantly improved, and the inter-cluster distance increases substantially.

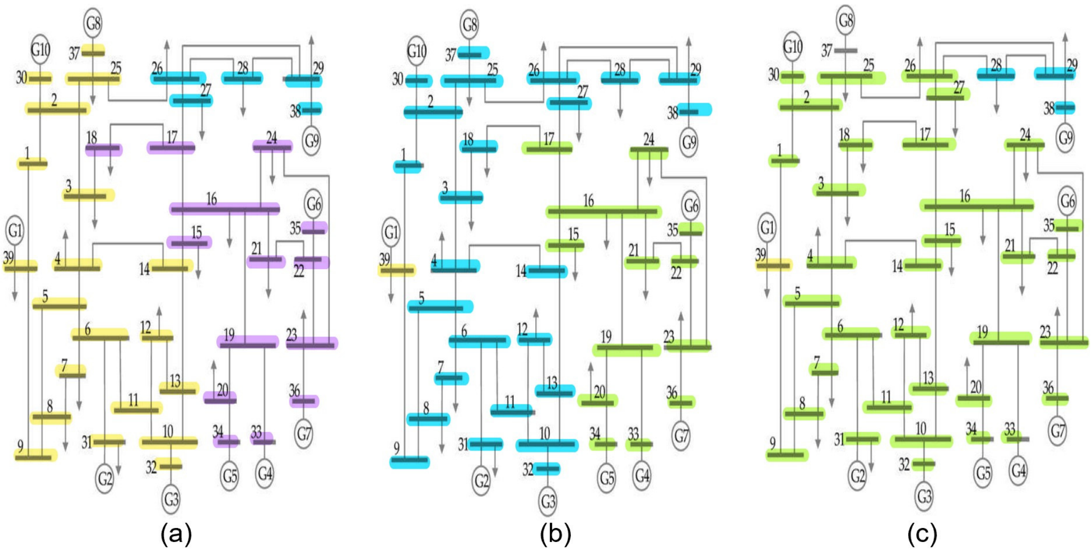

Figure 9. Three islanding solutions obtained from 100 runs of the CSC algorithm on the IEEE 39-bus system. Nodes with the same colour belong to the same island. The figure illustrates the variability of the CSC/k-medoids partitioning results; the dynamic performance of these three solutions is evaluated in Section 5.6.

The parameters used for the HIAC algorithm in this study were as follows:

- $x = 4$ (number of neighbours),
- $T = 0.5$ (motion time coefficient),
- $d = 100$ (number of time segments),
- and a threshold value of 0.80 for effective edge detection.

Using the ameliorated dataset of Figure 10b, the CSC algorithm was again executed 100 times, and in all executions, the algorithm returned the same islanding solution—corresponding to the configuration shown in Figure 9a. This confirms that the use of HIAC significantly improves clustering reliability, yielding a unique and stable islanding result.

It is also important to note that, for the case of generator coherency grouping (as discussed in Section 3.2), the clustering results were consistent across all 100 runs without the need for data amelioration. Hence, the HIAC algorithm was only applied to the bus-level spectral embedding, not to the generator-level clustering process.

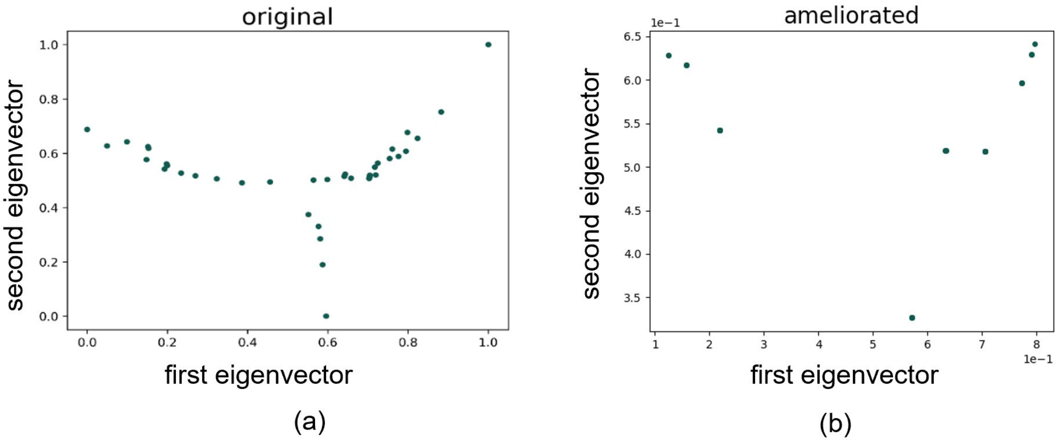

Figure 10. Spectral embedding of the IEEE 39-bus system in $\mathbb{R}^2$ before and after applying the HIAC algorithm. (**a**) Original spectral embedding with overlapping and poorly separated clusters. (**b**) Ameliorated embedding after HIAC application, showing improved compactness and inter-cluster separation.

It should be noted that the purpose of Figure 10 is not to benchmark HIAC using generic clustering validity indices, but to demonstrate its effect on the reliability of the CSC-based islanding process. In this case study, the relevant quantitative indicator is the reproducibility of the resulting islanding solution. Before data amelioration, repeated executions of CSC produced three different islanding configurations due to the random initialisation of k-medoids. After applying HIAC, the CSC algorithm was executed 100 times and returned the same islanding solution in all cases. This confirms that HIAC improves the stability of the clustering process and produces a unique islanding configuration, whose dynamic effectiveness is subsequently verified in Section 5.6.

HIAC Parameter Selection and Sensitivity Analysis

The HIAC procedure involves three main quantities: the number of nearest neighbours x, the motion-scaling parameter T, and the number of time segments d. In addition, the algorithm uses a threshold to distinguish valid neighbours from invalid neighbours. However, this threshold is not manually prescribed. It is obtained adaptively from the decision graph constructed from the object-weight probability distribution and is used to clip invalid edges from the topology graph. Therefore, the threshold is not treated as an independent tuning parameter in this study.

Among the HIAC parameters, x has the most direct influence on the construction of the topology graph, since it defines the initial set of nearest neighbours considered for each object. Consequently, it directly affects the valid-neighbour identification stage. In contrast, T and d are associated with the subsequent object-motion process. These parameters control the magnitude and number of gravitational movement steps after the valid-neighbour matrix has already been identified and locked. Thus, T and d affect the degree of data amelioration but do not redefine the valid-neighbour topology.

For this reason, the sensitivity analysis in this work focuses on x, which is the principal parameter governing neighbourhood construction. This is also consistent with the original HIAC formulation, where the decision-graph mechanism was shown to reduce the adverse effects of inappropriate x values by identifying and removing invalid edges. To assess the robustness of the proposed CSC-HIAC framework, the algorithm was tested using different values of x, while T and d were kept fixed for all simulations. Figure 11 shows the datasets ameliorated by the HIAC algorithm using different values of the neighbourhood-size parameter, namely $x = 5$, $x = 10$, $x = 15$, and $x = 20$. As observed, although a relatively wide range of x values is considered, the HIAC algorithm produces similar separation patterns in the ameliorated datasets. When each of these ameliorated datasets was used as input to the CSC algorithm, the same islanding solution was obtained in all cases, corresponding to the configuration shown in Figure 9a. Therefore, the results demonstrate that the final islanding solution remains consistent over the tested range of x, confirming that the proposed CSC-HIAC framework is not strongly sensitive to the selection of this parameter.

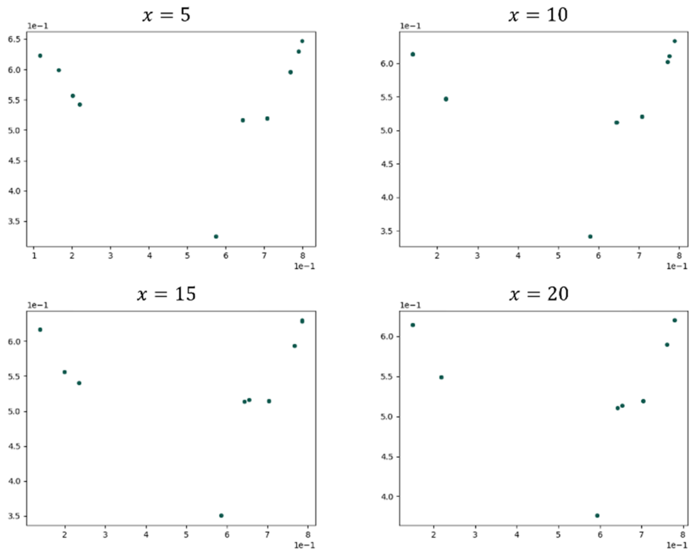

Figure 11. Spectral embedding of the IEEE 39-bus system in $\mathbb{R}^2$ after applying the HIAC algorithm with different x values. The similar separation patterns obtained for all tested values indicate that the CSC-HIAC framework is not strongly sensitive to the selection of neighbourhood-size parameter x.

5.6. Evaluation of Islanding Solutions for Mitigation of Cascading Failures for the IEEE 39-Bus System

To evaluate the effectiveness of the three islanding solutions shown in Figure 9, each configuration was tested under the cascading failure scenario initiated by the trip of Line 18 at $t = 10$ s. The dynamic simulations were conducted using the COSMIC simulator, and the resulting system responses are presented in Figure 12.

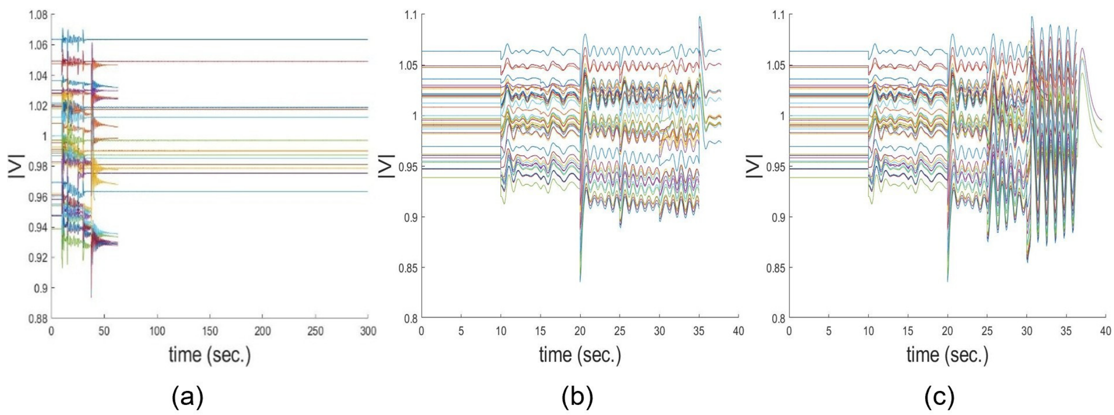

Figure 12. Dynamic simulation results for the fault at Line 18 under three different islanding solutions. (**a**) Simulation result with the islanding solution from Figure 9a, which successfully mitigates the cascading failure and avoids a blackout with partial load shedding of 3.833×10^3 MW. (**b**)

and (**c**) Simulation results with the islanding solutions from Figure 9b and 9c, respectively, both resulting in total blackouts with complete loss of the system load (6.1505 × 10^3 MW).

As shown in Figure 12a, the islanding solution of Figure 9a is the only configuration that successfully mitigates the cascading failure and prevents a total system blackout. Although some loads are shed during the separation process, the post-islanding system maintains dynamic stability. The total load shedding required in this case is approximately 3.833 × 10^3 MW—representing a significant improvement in system resilience compared to the uncontrolled case.

In contrast, the alternative islanding solutions shown in Figure 9b,c fail to prevent system collapse. As shown in Figure 12b,c, both islanding solutions result in total system blackouts, with complete loss of the system's total load (6.1505 × 10^3 MW). These results confirm two insights: (1) the clustering variability introduced by the random initialisation of the *k*-medoids algorithm can lead to significantly different islanding outcomes, where not necessarily all of them are able to suppress the cascade; and (2) the islanding solution (Figure 9a) obtained consistently with the ameliorated dataset, derived from the application of the HIAC algorithm, is effective in suppressing the cascade.

A second evaluation was conducted for the cascading failure scenario triggered by the trip of Line 31 at $t = 10$ s. The simulation results for the three islanding configurations are presented in Figure 13.

As shown in Figure 13a, the islanding solution of Figure 9a once again proves to be effective in mitigating the cascading failure. In this case, the system remains stable after separation, and a blackout is avoided. The required load shedding to maintain operational stability is 909.5 MW—substantially lower than in the previous case, and indicative of a well-balanced and resilient islanding solution.

In contrast, the solution corresponding to Figure 9b, whose results are displayed in Figure 13b, fails to contain the cascade. The system becomes unstable and collapses, resulting in a total blackout and the complete loss of load (6.1505 × 10^3 MW).

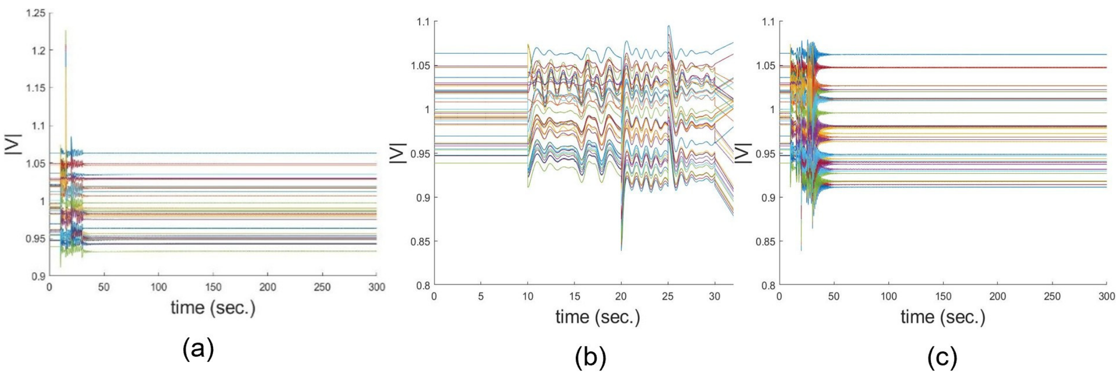

Figure 13. Dynamic simulation results for the fault at Line 31 under three different islanding solutions. (**a**) Simulation result with the islanding solution from Figure 9a, which mitigates the cascading failure with a load shedding of 909.5 MW. (**b**) Simulation result with the islanding solution from Figure 9b, which fails to prevent the blackout. (**c**) Simulation result with the islanding solution from Figure 9c, which also avoids blackout but requires a higher load shedding of 1.5935 × 10^3 MW.

Interestingly, the third solution—shown in Figure 13c, corresponding to the islanding solution of Figure 9c—is also able to prevent a blackout. However, the required load shedding in this case amounts to 1.5935 × 10^3 MW, which is significantly higher than that of the solution of Figure 9a, the one obtained consistently with the ameliorated dataset. These results indicate that although more than one islanding configuration may stabilise the system, the application of the HIAC technique leads to a solution that not only

https://doi.org/10.3390/sym18071196

preserves dynamic stability but also achieves a lower system disruption cost, as measured by the amount of load curtailed. This could also inform the fine tuning of the load shedding strategies.

Although the proposed CSC-HIAC framework is evaluated using the IEEE RTS-96 three-area system and the IEEE 39-bus system, its applicability is not restricted to these networks. These systems were selected because they are widely used benchmark systems in the ICI literature and because they provide different structural characteristics for testing the proposed method. The RTS-96 system offers a modular and relatively symmetric multi-area structure, whereas the IEEE 39-bus system presents a more intricate topology and a less straightforward clustering structure. Therefore, the two systems provide complementary test conditions for assessing the proposed framework.

Nevertheless, further validation is required before practical deployment in large-scale power systems. In particular, future studies should consider larger and more realistic networks, different loading conditions, high penetration of renewable generation, uncertainty in operating conditions, and a wider range of cascading failure scenarios. Since the proposed framework is designed for the Offline Analysis stage of ICI, where candidate islanding boundaries are determined in advance, its computational requirements are less restrictive than those of real-time control actions. This makes the framework suitable for further extension to larger systems, although additional scalability-oriented studies remain necessary.

6. Limitations of the Proposed Framework

Although the proposed CSC-HIAC framework provides an effective approach for determining islanding boundaries and validating their dynamic performance, several limitations should be acknowledged. First, the framework is mainly designed for the Offline Analysis (OFA) stage of ICI, where the question of where to island is addressed by identifying suitable separation boundaries in advance. Therefore, the present study does not explicitly model practical issues associated with online monitoring and real-time control, such as communication delays, data latency, or the coordination time of separation relays. In practical applications, these factors may affect the timely activation of the selected islanding strategy.

Second, the proposed framework assumes that the information required for coherency identification and islanding-boundary determination is available with sufficient accuracy. However, in real power systems, PMU measurements may be affected by noise, missing data, synchronisation errors, or communication failures. These issues can influence the accuracy of modal information, coherency assessment, and real-time decision-making. Although the islanding boundaries are determined offline in the proposed framework, the practical triggering and execution of ICI would require robust monitoring and control mechanisms capable of handling measurement uncertainty.

Third, the present framework focuses on determining suitable islanding boundaries during the OFA stage and does not explicitly optimise post-islanding corrective controls. Therefore, load shedding in the dynamic simulations should be interpreted as the corrective action required to preserve feasible post-islanding operation under the simulated cascading failure conditions. Further reductions in load curtailment may be achieved by integrating the proposed CSC-HIAC framework with post-islanding control strategies, such as optimal load shedding, generation redispatch, voltage support, and adaptive frequency-control mechanisms. The development of such coordinated islanding and post-islanding control schemes is left for future work.

Fourth, the present study does not explicitly consider high renewable energy penetration or the uncertainty associated with converter-interfaced generation. Renewable generation can modify power flow patterns, reduce system inertia, alter generator coherency behaviour, and increase operating-condition variability. These effects may influence both the selection of islanding boundaries and the post-islanding dynamic response. Therefore, additional studies are required to evaluate the proposed CSC-HIAC framework under renewable-rich and uncertainty-aware operating conditions.

Finally, although the proposed method has been validated using the IEEE RTS-96 three-area system and the IEEE 39-bus system, further testing on larger and more complex networks is required before practical deployment. Large-scale implementation should consider broader sets of operating points, contingency scenarios, loading levels, protection actions, and dynamic models. Since the proposed approach is intended for the OFA stage, its computational requirements are less restrictive than those of real-time control schemes; nevertheless, scalability-oriented studies remain necessary to confirm its applicability to practical large-scale power systems.

7. Conclusions

Intentional Controlled Islanding (ICI) has emerged as a crucial strategy to prevent large-scale blackouts in power systems by partitioning the grid into dynamically stable and operationally viable islands during cascading failures. Recent contributions in the literature have focused on achieving this objective by ensuring that each island contains only coherent generators while minimising the disruption of power flows. Among these methods, approaches based on constrained spectral clustering (CSC) have shown significant promise.

CSC techniques typically rely on conventional clustering algorithms, such as k-medoids, to group nodes in a reduced-dimensional space. However, these algorithms exhibit well-documented limitations—such as sensitivity to initialisation and poor performance with overlapping or poorly separated clusters—which can compromise the robustness and accuracy of islanding solutions. To address these challenges, this study proposed a novel ICI framework that integrates a data amelioration technique known as HIAC. This method enhances the compactness and separability of clusters, thereby improving the consistency and reliability of the clustering results.

In addition to the methodological contribution, the proposed ICI framework includes a validation phase based on dynamic cascading failure simulations, performed using the open-access COSMIC simulator. The framework was applied to two benchmark systems: the IEEE RTS-96 three-area system and the IEEE 39-bus system.

In the RTS-96 test case, the system's modular and self-sufficient structure enabled the CSC algorithm to consistently identify stable and coherent islands without the need for data amelioration. The resulting islanding actions effectively mitigated cascading failures and prevented complete blackouts, demonstrating the framework's applicability under favourable clustering conditions.

In contrast, the IEEE 39-bus system posed a greater challenge due to its complex and non-modular topology. In this case, the direct application of CSC produced inconsistent clustering results. However, by incorporating the HIAC technique, the clustering process yielded a unique and stable islanding solution. This improved solution not only preserved system stability during cascading failures but also reduced the overall system disruption cost in terms of load curtailed.

With respect to the computational cost and scalability of the proposed framework, compared with standard CSC, the CSC-HIAC framework introduces an additional data amelioration stage before the final clustering step. The computational cost of this stage is $O(xN + dsN)$, where x is the number of nearest neighbours considered for each object, d is the number of movement iterations, and s is the average number of valid neighbours, with $s < x$. For fixed x, d, and s, this additional cost grows approximately linearly with the number of objects. Therefore, the integration of HIAC does not change the dominant computational order of the CSC-based islanding framework, which remains governed by the eigen decomposition step of the constrained spectral clustering procedure. Since the proposed method is intended for the Offline Analysis stage, where islanding boundaries are determined in advance, strict real-time execution constraints are not imposed. Further execution-time benchmarking on larger systems, such as IEEE 118-bus and IEEE 300-bus networks, will be considered in future work.

In summary, the proposed CSC-based ICI framework, enhanced by data amelioration and validated through dynamic simulation, provides a robust, reproducible, and effective approach for identifying critical islands in power systems. It adapts well to system topologies of varying complexity and supports real-time decision-making to improve grid resilience, improvement of load shedding strategies, and preparing the system for timely restoration efforts.

Future work will extend the proposed CSC-HIAC framework to larger and more complex power systems, including networks with high renewable generation penetration and uncertain operating conditions. Additional cascading failure scenarios, loading levels, and dynamic operating conditions will also be considered to further assess the scalability, robustness, and practical applicability of the proposed islanding strategy.

In addition, future research will investigate AI-assisted islanding strategies, adaptive clustering mechanisms capable of updating islanding boundaries under changing operating conditions, PMU-based real-time implementation for online monitoring and triggering, and digital-twin-assisted environments for testing, validating, and refining the proposed framework before field deployment.

Author Contributions: F.R.-D. made substantial contributions to the conception of the work. P.G.-P. and E.C.-S. made substantial contributions to the creation of new software used in the work. S.M. and M.M.-M. revised it critically for important intellectual content. All authors made substantial contributions to the acquisition, analysis, and interpretation of data. All authors agree to be accountable for all aspects of the work in ensuring that questions related to the accuracy or integrity of any part of the work are appropriately investigated and resolved. All authors have read and agreed to the published version of the manuscript.

Funding: The authors declare no funding was received for conducting this study.

Data Availability Statement: The original contributions presented in this study are included in the article. Further inquiries can be directed to the corresponding author.

Acknowledgments: Paulina García-Peña gratefully acknowledges the National Council of Humanities Science and Technology (CONAHCYT) for the scholarship granted. During the preparation of this manuscript, the authors used ChatGPT version 5.0 for the purposes of text editing, including grammar, spelling, punctuation, and formatting corrections. The authors have reviewed and edited the output and take full responsibility for the content of this publication.

Conflicts of Interest: The authors declare they have no relevant financial or non-financial interests to disclose.

References

1. Zakaria, R. Are We Entering an Age of Increasing Power Supply Disruptions? January 2022. Available online: https://www.spglobal.com/commodity-insights/en/research-analytics/are-we-entering-an-age-of-increasing-power-supply-disruptions (accessed on 10 February 2025).
2. Khattak, M.A.; Yahya, T.M.; Sallehhudin, M.W.; Ghazali, M.I.; Abdullah, N.A.; Nordin, N.A.; Dzakurnain, N.A. Energy Security Policy Shift of North America and Ontario, Canada Following 2003 Power Blackout: A Review. *Prog. Energy Environ.* **2018**, *4*, 14–24.

3. Yang, B.; Vittal, V.; Heydt, G. Slow-coherency-based controlled islanding—A demonstration of the approach on the August 14, 2003 blackout scenario. *IEEE Trans. Power Syst.* **2006**, *21*, 1840–1847.
4. Sun, K.; Hur, K.; Zhang, P. A new unified scheme for controlled power system separation using synchronized phasor measurements. *IEEE Trans. Power Syst.* **2011**, *26*, 1544–1554.
5. Amini, M.; Samet, H.; Seifi, A.R.; Al-Dhaifallah, M.; Ali, Z.M. An effective multi-solution approach for power system islanding. *IEEE Access* **2020**, *8*, 93200–93210.
6. Kyriacou, A.; Demetriou, P.; Panayiotou, C.; Kyriakides, E. Controlled islanding solution for large-scale power systems. *IEEE Trans. Power Syst.* **2017**, *33*, 1591–1602.
7. Esmaeilian, A.; Kezunovic, M. Controlled islanding to prevent cascade outages using constrained spectral k-embedded clustering. In *2016 Power Systems Computation Conference (PSCC)*; IEEE: Piscataway, NJ, USA, 2016; pp. 1–6.
8. Tyuryukanov, I.; Karagiannis Kaltsikis, A.C.; Popov, M.; van der Meijden, M.A.; Terzija, V. Generator grouping cutset determination based on tree construction and constrained spectral clustering. *J. Eng.* **2018**, *2018*, 1309–1314.
9. You, H.; Vittal, V.; Yang, Z. Self-healing in power systems: An approach using islanding and rate of frequency decline-based load shedding. *IEEE Trans. Power Syst.* **2003**, *18*, 174–181.
10. Sun, K.; Zheng, D.Z.; Lu, Q. Splitting strategies for islanding operation of large-scale power systems using OBDD-based methods. *IEEE Trans. Power Syst.* **2003**, *18*, 912–923.
11. Zhao, Q.; Sun, K.; Zheng, D.Z.; Ma, J.; Lu, Q. A study of system splitting strategies for island operation of power system: A two-phase method based on OBDDs. *IEEE Trans. Power Syst.* **2003**, *18*, 1556–1565.
12. You, H.; Vittal, V.; Wang, X. Slow coherency-based islanding. *IEEE Trans. Power Syst.* **2004**, *19*, 483–491.
13. Xu, G.; Vittal, V. Slow coherency based cutset determination algorithm for large power systems. *IEEE Trans. Power Syst.* **2009**, *25*, 877–884.
14. Wang, C.G.; Zhang, B.H.; Hao, Z.G.; Shu, J.; Li, P.; Bo, Z.Q. A novel real-time searching method for power system splitting boundary. *IEEE Trans. Power Syst.* **2010**, *25*, 1902–1909.
15. Sun, K.; Zheng, D.Z.; Lu, Q. A simulation study of OBDD-based proper splitting strategies for power systems under consideration of transient stability. *IEEE Trans. Power Syst.* **2005**, *20*, 389–399.
16. Li, H.; Rosenwald, G.W.; Jung, J.; Liu, C.C. Strategic power infrastructure defense. *Proc. IEEE* **2005**, *93*, 918–933.
17. Ding, L.; Gonzalez-Longatt, F.M.; Wall, P.; Terzija, V. Two-step spectral clustering controlled islanding algorithm. *IEEE Trans. Power Syst.* **2012**, *28*, 75–84.
18. Von Luxburg, U. A tutorial on spectral clustering. *Stat. Comput.* **2007**, *17*, 395–416.
19. Quirós - Tortós, J.; Sánchez - García, R.; Brodzki, J.; Bialek, J.; Terzija, V. Constrained spectral clustering-based methodology for intentional controlled islanding of large-scale power systems. *IET Gener. Transm. Distrib.* **2015**, *9*, 31–42.
20. Salama, M.; El-Dakhakhni, W.; Tait, M. Systemic risk mitigation strategy for power grid cascade failures using constrained spectral clustering. *Int. J. Crit. Infrastruct. Prot.* **2023**, *42*, 100622.
21. Massaoudi, M.; Eddin, M.E.; Ghrayeb, A.; Abu-Rub, H.; Refaat, S.S. Advancing coherent power grid partitioning: A review embracing machine and deep learning. *IEEE Open Access J. Power Energy* **2025**, *12*, 59–75.
22. Wang, R.; Bu, S.; Zhu, Z.; Li, G. Deep Reinforcement Learning for Intentional Controlled Islanding of Power Systems. *IEEE Trans. Ind. Inform.* 2026, *Early Access*. https://doi.org/10.1109/TII.2026.3688145.
23. Badakhshan, S.; Jacob, R.A.; Li, B.; Wang, P.; Zhang, J. Self-healing power systems using reinforcement learning over graphs for controlled grid islanding. *Sustain. Energy Grids Netw.* **2025**, *44*, 101937.
24. Huang, Y.; Gao, C.; Lu, H.; Xin, Z.; Li, G.; Bie, Z. Risk-triggered preventive islanding for cascading failure mitigation and resilience enhancement in typhoon-prone power systems. *Int. J. Electr. Power Energy Syst.* **2025**, *173*, 111422.
25. Liu, J.; Han, J. Spectral clustering. In *Data Clustering*; Chapman and Hall/CRC: Boca Raton, FL, USA, 2018; pp. 177–200.
26. Tyuryukanov, I. Graph Partitioning Algorithms for Control of AC Transmission Networks: Generator Slow Coherency, Intentional Controlled Islanding, and Secondary Voltage Control. Ph.D. Thesis, Delft University of Technology, Delft, The Netherlands, 2020. https://doi.org/10.4233/uuid:a2c1a54a-ab89-4a6a-b9f9-c63241d2c4b8.
27. Alswaitti, M.; Ishak, M.K.; Isa, N.A.M. Optimized gravitational-based data clustering algorithm. *Eng. Appl. Artif. Intell.* **2018**, *73*, 126–148.
28. Li, Q.; Wang, S.; Zhao, C.; Zhao, B.; Yue, X.; Geng, J. HIBOG: Improving the clustering accuracy by ameliorating dataset with gravitation. *Inf. Sci.* **2021**, *550*, 41–56.
29. Wang, X.X.; Zhang, Y.F.; Xie, J.; Dai, Q.Z.; Xiong, Z.Y.; Dan, J.P. A density-core-based clustering algorithm with local resultant force. *Soft Comput.* **2020**, *24*, 6571–6590.

30. Wang, Z.; Yu, Z.; Chen, C.P.; You, J.; Gu, T.; Wong, H.S.; Zhang, J. Clustering by local gravitation. *IEEE Trans. Cybern.* **2017**, *48*, 1383–1396.
31. Wong, K.C.; Peng, C.; Li, Y.; Chan, T.M. Herd clustering: A synergistic data clustering approach using collective intelligence. *Appl. Soft Comput.* **2014**, *23*, 61–75.
32. Xie, J.; Xiong, Z.; Dai, Q.; Wang, X.; Zhang, Y. A local-gravitation-based method for the detection of outliers and boundary points. *Knowl.-Based Syst.* **2020**, *192*, 105331.
33. Li, Q.; Wang, S.; Zeng, X.; Zhao, B.; Dang, Y. How to improve the accuracy of clustering algorithms. *Inf. Sci.* **2023**, *627*, 52–70.
34. Song, J.; Cotilla-Sanchez, E.; Ghanavati, G.; Hines, P.D. Dynamic modeling of cascading failure in power systems. *IEEE Trans. Power Syst.* **2015**, *31*, 2085–2095.
35. Wang, X.; Qian, B.; Davidson, I. On constrained spectral clustering and its applications. *Data Min. Knowl. Discov.* **2014**, *28*, 1–30.